

Graphene sheets stacked polyacrylate latex composites for ultra-efficient electromagnetic shielding

This content has been downloaded from IOPscience. Please scroll down to see the full text.

2016 Mater. Res. Express 3 075012

(<http://iopscience.iop.org/2053-1591/3/7/075012>)

View the [table of contents for this issue](#), or go to the [journal homepage](#) for more

Download details:

IP Address: 132.239.1.231

This content was downloaded on 24/07/2016 at 16:12

Please note that [terms and conditions apply](#).

Materials Research Express



PAPER

RECEIVED
29 March 2016

ACCEPTED FOR PUBLICATION
31 May 2016

PUBLISHED
21 July 2016

Graphene sheets stacked polyacrylate latex composites for ultra-efficient electromagnetic shielding

Yong Li¹, Song Zhang² and Yuwei Ni²

¹ Key Laboratory of Cryogenics, Technical Institute of Physics and Chemistry, Chinese Academy of Sciences, Beijing 100190, People's Republic of China

² Navy Logistic Technology and Equipment Institute of PLA, Beijing, 100072, People's Republic of China

E-mail: liyong1897@163.com

Keywords: graphene sheets, polyacrylate latex, electromagnetic shielding, percolation threshold

Abstract

Graphene sheets (GS) are at the forefront of electromagnetic interference (EMI) shielding/attenuation materials science research because of their excellent electrical properties (Wen B *et al* 2014 *Adv. Mater.* **26** 3484, Zhang Y *et al* 2015 *Adv. Mater.* **27** 2049). GS/polyacrylate (PA) composites were prepared using a solvent-free latex technology, which favored the build-up of a segregated GS architecture stacked in the polymer matrix. GS were obtained from graphite flakes (GF) via a mechanical delamination approach in water. The microstructure, electrical, dielectric and electromagnetic shielding properties of the GS/PA composites were correlated in this manuscript. A remarkably low percolation threshold of ~0.11 mass per cent for room-temperature electrical conductivity was obtained in the GS/PA composites owing to the stacked architecture of GS with high aspect ratios. This unique nanostructured GS architecture not only enhanced the electrical conductivity of composites, but also dramatically increased complex permittivity by inducing strong Maxwell–Wagner–Sillars (MWS) polarization at the highly conductive GS/non-conductive PA interfaces. The EMI shielding effectiveness (SE) of these composites was enhanced with increasing GS content, and the composite with 6 wt% GS loading exhibited a high EMI SE of ~66 dB over a frequency of 8.2–12.4 GHz, resulting from the pronounced conduction loss, dielectric relaxation, and multi-scattering.

Introduction

The widespread use of gigahertz electronic devices, from local area wireless network, satellite communications, to military radar surveillance systems, etc is responsible for steadily increasing electromagnetic emission problems in our everyday lives, which may degrade the performance of other devices or harm human health [3]. Many diseases such as leukemia, miscarriages, etc are correlated to continuous exposure to microwave irradiation and pulses [4–6], and the World Health Organization (WHO) has raised its concerns over excessive EM emissions in our environment [7]. Maintenance of EMI shielding and EM compatibility by utilizing various functional materials has become an imperative, especially in areas of residences and workplaces. For those applications, the materials must be sustainable, lightweight, flexible and fully compatible with building substrates, such as concrete. Moreover, the measurement for EMI performance is also different from those applied in electromagnetic compatibility. Compared with metal-based EMI shielding materials, composites containing carbon-based nanofillers are becoming attractive because of their light weight, high chemical stability, low cost and excellent adaptability to a wide range of environments [8].

The EMI shielding performance of a carbon-based composite primarily depends on the intrinsic electrical conductivity, aspect ratio, and loading of the fillers [9]. Mono- and multilayer graphene sheets (GS), composed of 2D honeycomb lattices of carbon atoms, have recently attracted much attention as a filler for polymer-based microwave shielding/attenuation nanocomposites due to their high electrical conductivity and aspect ratios,

excellent mechanical strength and flexibility [10, 11]. Moreover, GS are highly desirable as an EM wave absorber because of their high aspect ratios, large interfaces, high dielectric loss and low density [12–14].

In most GS-polymer composites studied, the polymer was optimized to exfoliate or at least to disperse the GS due to the poor compatibility of GS. Therefore, most reported GS-based composites consisted either of polymers that have been specially synthesized to disperse the GS [15, 16], or, alternatively the GS were functionalized to enhance the compatibility with the polymer [17]. The former method introduced serious limitations on the spectrum of target polymer matrices, while the latter may lead to deterioration of some properties (e.g. conductivity) of bare GS. Moreover, the architecture of GS in the polymer matrix cannot be tuned by the polymer in the above two approaches. Recently, composites with 3D segregated filler networks have been constructed in the composites by distributing low concentrations of carbon nanotubes (CNTs) or GS at the boundaries between the polymer spheres using a solvent-free latex blending technology [18, 19]. Compared with traditional melt or organic solution routes, the latex blending route can exhibit two major advantages. First, this preparation route is sustainable and environmentally friendly as latex is made of polymer spheres in an aqueous suspension without using organic solvent; second, the polymer used in the latex route can not only disperse GS, but also favor the build-up of a tunable architecture of GS in the polymer matrix [18].

PA latex is widely used in the field of the architectural paints for its prominent properties such as high resistance to UV light, oxygen, water, various types of solvents and excellent durability [20]. However, pure PA polymer is non-conductive and provides no shielding property, which motivated us to construct a segregated GS architecture in PA matrix to prepare high performance EMI shielding composites.

In the present report, we demonstrate a promising green approach to fabrication of ultra-efficient electromagnetic shielding GS/PA composites with low active filler loading, high conductivity and complex permittivity. GS were obtained from GF via a mechanical delamination approach in water. The composites were prepared by stacking a segregated GS architecture in the PA matrix using a solvent-free latex blending technology. A high room-temperature electrical conductivity ($\sim 190 \text{ S m}^{-1}$) and remarkable low percolation threshold of ~ 0.11 mass per cent were obtained in the GS/PA composites. Microwave measurement showed GS/PA composites had high complex permittivity owing to the strong MWX polarization. The GS/PA composites with 6 wt% loading exhibited a high EMI shielding effectiveness (SE) of ~ 66 dB over a frequency of 8.2–12.4 GHz, resulting from the pronounced conduction loss, dielectric relaxation, and multi-scattering.

Experimental and characterization

Materials

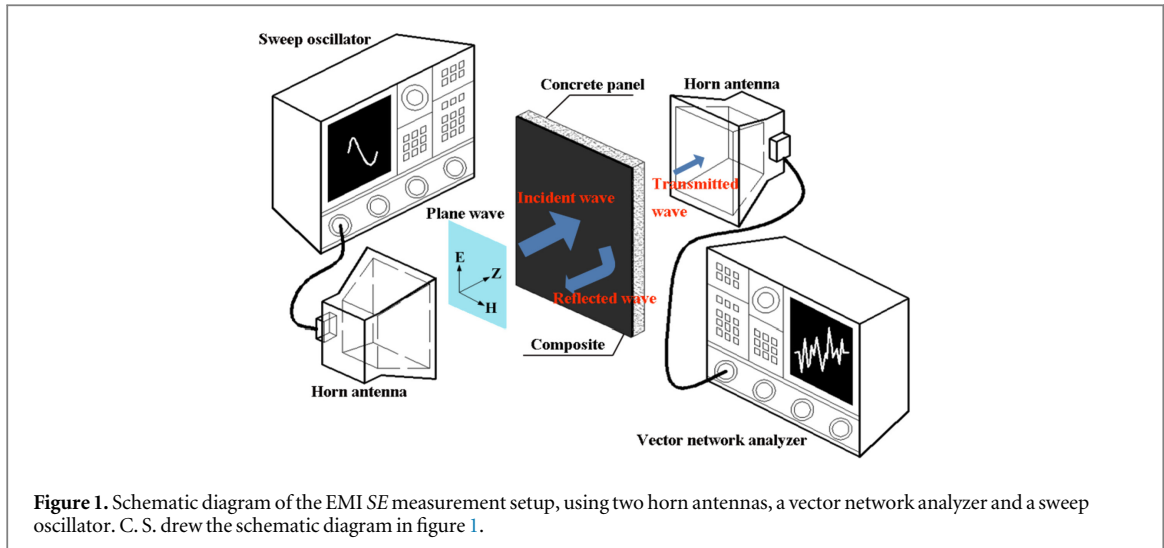
PA latex (Beijing Huyi Co., Ltd., 55 wt% solid content) with a latex sphere diameter of 500 nm, was used as received. The minimum film formation temperature for this latex is 15 °C, and the glass transition temperature (T_g) is 34 °C. GF (Alfa Aesar, 99.99% Purity) with a mean particle size of 4 μm , and sodium dodecyl sulfate (SDS, Alfa Aesar) were used as received.

Preparation of graphene sheets (GS)

The starting point of composite fabrication was the preparation of exfoliated GS aqueous dispersions, which were prepared from GF using a wet grinding process under mild milling conditions as reported elsewhere [18]. Typically, the GF (100 g) and SDS (2 g) were dispersed in deionized water (500 ml) via sonication dispersion (140 W) for 4 h until a dark brown solution was obtained. The solution was further ground in a vertical laboratory stirred media mill (PE075, Netzsch Feinmahltechnik GmbH, Selb, Germany) for 6 h at 1200 rpm. In the grinding process, Yttrium-stabilized zirconium oxide grinding beads with diameter of 100 μm were used as grinding media. A sonicator was added in the attritor loop to improve graphite exfoliation and scission. The resulting GS suspension was then centrifuged to isolate possible large graphite particles. About 30% graphite material was lost during this step and remained in the residue of the centrifugation. The GS suspensions were used as-is and the GS concentrations in the suspensions were determined by subtracting the mass of large graphite particles.

Preparation of the GS/PA composites

The latex mixing process described below was used to prepare the composites. The GS suspensions were added to SDS-stabilized PA latex in an ultrasonic bath to favor the adsorption of GS on the surface of latex spheres. The colloidal mixtures were sonicated for 4 h to obtain homogeneous black solution. The highest concentration of GS in the suspension was prepared first, and lower concentrations were obtained by diluting the mixture with more latex and deionized water. After the above mixing process, the suspensions were allowed to equilibrate for 24 h. During this process, the solid polymer particles can create an excluded volume and push the nanosized GS into the interstitial space between them. Attractive depletion interactions between the GSs were caused by the



presence of the spherical latex particles in the mixture and a self-assembled GS network was formed as a result of the reversible aggregation of colloidal PA spheres driven by thermodynamics [21].

The prepared suspensions were then spin-coated onto concrete panels ($60\text{ cm} \times 60\text{ cm} \times 5\text{ cm}$), and dried at ambient temperature (25°C). Concrete panels were prepared in our laboratory with ordinary cement, coarse aggregate and natural sand (1:2:4). Composites with different GS and GF mass fractions were fabricated.

Characterization

The surface morphology of the as-prepared GS and GS/PA composites was observed using a field-emission scanning electron microscope (FESEM HITACHI S-4300) at an accelerating voltage of 5 kV. The composites were freeze-fractured in liquid nitrogen and the fractured surface was coated with a thin layer of gold before observation. The detailed morphology of as-prepared GS was also observed by transmission electron microscopy (TEM, JEOL-2010). The GS dispersion was ultrasonicated for 1.5 h and dropped onto standard TEM grids and dried in air. Atomic force microscopy (AFM) images were taken on a MultiTask AutoProbe CP/MT Scanning Probe Microscope (Veeco Instruments, Woodbury, NY). Samples for AFM imaging were prepared by depositing GS suspension on freshly cleaved mica surface (Ted Pella Inc.) and allowing them to dry in air. The dc conductivity of the composites was measured with an ESCORT apparatus of resistance Model 3146A coupled with a four point cylindrical probe on rectangular concrete slabs. Data was taken as the average of at least three measurements. The scattering parameters (S_{11} and S_{12}) of the prepared GS/PA and GF/PA samples with different filler mass fractions were measured by an HP vector network analyzer (HP 8563E) using a waveguide method. Before measurement, GS/PA and GF/PA composite slabs of dimension $22.86\text{ cm} \times 10.16\text{ cm} \times 2\text{ cm}$ were prepared to fit the waveguide sample holder. The relative complex permittivity ($\epsilon = \epsilon' + i\epsilon''$) was extracted from scattering parameters using the Son-Ross-Weir method [22].

The SE of the flexible, thin composites was measured by a carefully designed measurement system based on modified MIL-STD-285 (Military Standard Attenuation Measurements for Enclosures, Electromagnetic Shielding, for Electronic Test Purposes). The experimental set-up, sketched in figure 1, is mainly composed of a vector network analyzer (Hewlett Packard HP 8563E), a sweep oscillator (Hewlett Packard HP83640A), two horn antennas and a concrete panel with composite sample. An anechoic shielded room ($>120\text{ dB}$) with wedge-shaped microwave absorbers on the inside wall, was used to isolate the measurement environment from all other external EMI (figure S1). The EMI SE is derived from the data of incident (P_{inc}) and transmitted (P_{trans}) power according to the following equation:

$$SE_{\text{total}} = 10 \log(P_{\text{inc}}/P_{\text{trans}}). \quad (1)$$

In order to exclude the effects of the concrete panel, the SE of a concrete panel with no composite films was measured first, and the result used as the SE reference level. The frequency was scanned from 8.2 to 12.4 GHz (X-band) and 12 data points were taken. This frequency range is quite important for applications like TV signal transmission, Doppler, radar systems, etc.

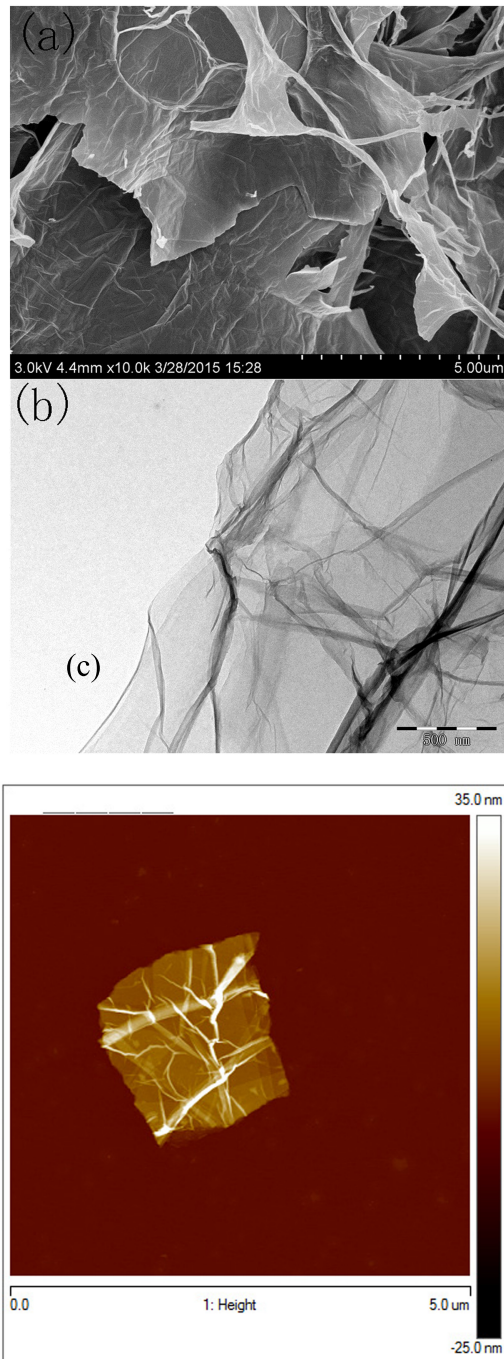


Figure 2. SEM (a) and TEM (b) and AFM (c) of the as-prepared GS.

Results and discussions

Microstructural characterization

The as-prepared GS resulting from the suspensions was characterized by SEM imaging in charge contrast mode. According to the SEM results in low (figure S2) and high (figure 2(a)) magnifications, Mono- and multilayer highly delaminated GSs are stacked and partially folded, and the lateral size (edge to edge) of the GS are on the order of several microns. Figure 2(b) shows the TEM image of the prepared GS, which exhibit typical transparent and slightly rippled features, indicating the unique few-layered structure featuring large aspect ratio. AFM was used to investigate the thickness of the GS. The AFM image shown in figure 2(c) revealed the presence of curled and thin wrinkled sheets. Therefore, the combined results from SEM, TEM and AFM suggested that the aspect ratios of the exfoliated GS via a mechanical delamination approach are on the order of 100 and higher, in the same order of magnitude as those prepared by other techniques [1, 10].

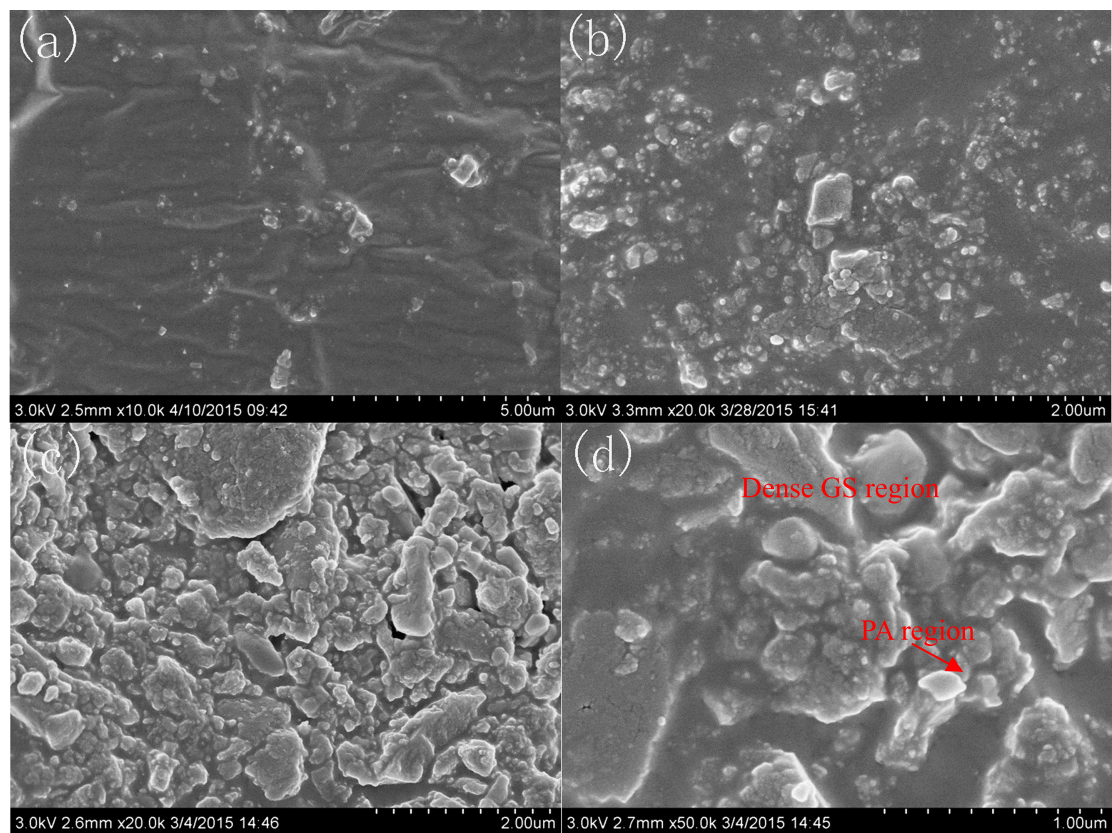


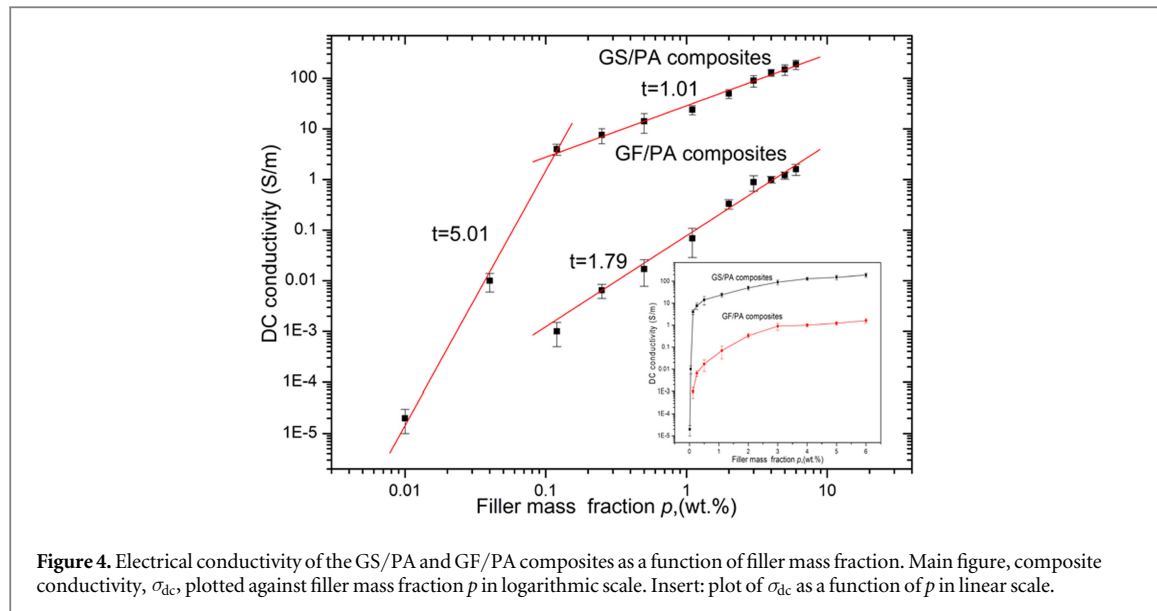
Figure 3. Cross-sectional SEM images of the freshly fractured surfaces of GS/PA composites with different GS loadings: (a) 0.12 wt%, (b) 1.1 wt%, and (c) 4.0 wt% and (d) high magnification of (c) imaging in charge contrast mode.

It has been shown that the dispersion of the nanofiller in the polymer matrix directly correlates with its performance in enhancing mechanical, electrical, thermal, and other properties of polymer-based nanocomposites [23, 24]. The dispersion of GS in the PA matrix was characterized by SEM imaging (figure 3) for 0.12, 1.1 and 4 wt% GS loadings respectively. The morphology of layer-structured GS can easily be identified even at a GS loading as low as 0.12 wt%, which can be ascribed to large specific surface area ($\sim 2600 \text{ m}^2 \text{ g}^{-1}$ for an individual graphene sheet) and strong contrast with insulating PA matrix due to enriched secondary electron yield at the location of the GS. SEM images of GS/PA composites showed clearly that the segregated architecture of GS was uniformly stacked in the PA matrix and the density of GS proportionally increased with GS loading. The SEM image of the composite containing 4 wt % GS shows an interface with densely stacked GS (figures 3(c), (d)). The presence of the PA latex spheres in the suspensions was a key for stacking GS in the PA matrix. As the latex mixing proceeded, the GS became covered with deformed PA spheres and remain individually dispersed. The latex particles deformed and fused together during the process of composite film formation, facilitating the build-up of a segregated architecture of GS in the PA matrix. Moreover, the construction of such a well-developed interconnected GS network can generate pathways for charge carrier transport in the composites.

Electrical conductivity

Electrical conductivity is critical for EMI shielding performance, for it is intrinsic to the ability of EMI shielding materials in reflecting and absorbing electromagnetic emissions. The electrical conductivity of the EMI shielding composite can increase over 10^{10} times compared to the parent polymer [23–25]. The influence of GS content on the dc conductivity of GS/PA composite was investigated. As a comparison, GF/PA composites were prepared at the same filler concentrations. Figure 4 exhibits the dc electrical conductivity (σ_{dc}) of GS/PA and GF/PA composites as a function of filler mass fractions in logarithmic scale. For GS/PA composites, the σ_{dc} rose quickly to 4 S m^{-1} from $2 \times 10^{-5} \text{ S m}^{-1}$ with a slight increase in GS mass loading from 0.01 to 0.12 wt%, demonstrating an obvious percolation behavior. Percolation is defined as the sudden increase of conductivity at a critical filler concentration (ϕ_c) where the conductive nanofillers are in close enough proximity to generate a pathway for charge carrier transport [26].

The electrical percolation behavior follows a scaling law around the percolation threshold [27], as shown in equation (2):



$$\sigma \propto |\phi - \phi_c|^t \quad (2)$$

Where σ is the composite conductivity, ϕ is the filler volume fraction, ϕ_c is the percolation threshold volume fraction, t is the critical exponent. The mass fraction (p) of GS is preferred instead of the volume fraction (ϕ) due to the similarity between p and ϕ of GS. Figure 4 showed that the conductivity of GS/PA composites agreed well with the scaling law. The slope, i.e., the critical exponent t in equation (2) varied from 5.01 to 1.01, implying a low conductivity percolation threshold at $p \sim 0.11$ wt%. The low percolation value of the prepared GS/PA composite compared well with the lowest values reported in the literature for graphene–polymer composites [24, 25]. At 0.12 wt% GS, the electrical conductivity of GS/PA composites was ~ 4 S m $^{-1}$, which is a sufficient level of conductivity for many electrical applications including EMI shielding [24, 28, 29]. The maximum conductivity of ~ 190 S m $^{-1}$ was achieved for the GS/PA composite with 6 wt% GS loading. The high dc conductivity and low threshold value were ascribed to the highly intrinsic conductivity of GS and the formation of a segregated architecture of GS in the PA matrix. Compared with the GS/PA composite, GF/PA composite exhibited a lower conductivity at the same filler loading. The critical exponent t is ~ 1.79 and can be expected to change at higher filler loading (> 6 wt %) from the conductivity configuration.

Dielectric properties

It has been shown that high permittivity is crucial for composites with electrically conductive or dielectric fillers to raise microwave absorption capacity [30]. The complex permittivity of the as-prepared composites, which was extracted from the S-parameters, was investigated. The real (ϵ') and imaginary (ϵ'') permittivity of the GS/PA and GF/PA composites, representing polarization loss and electric loss respectively, were shown in figure 5. The permittivity of pure PA polymer and composite made from 5 wt % GF were given for comparison. The observed ϵ' and ϵ'' of the GS/PA composite exhibited a rapid increase as the mass concentration of the GS increased from 0.12 to 6.0 wt%, and the increase was more remarkable when the mass fraction was larger than the percolation threshold (0.11 wt%). The real permittivity lines for the 0.12, 1.0 and 3.0 wt% GS loaded samples were relatively flat, whereas the lines for the 4.0, 5.0 and 6.0 wt% GS loaded samples decreased with increasing frequency, exhibiting a frequency-dependent dielectric response (figure 5(a)). Such behaviors were due to the lag of induced electric field in response to the reversing external electrical field at high frequencies, resulting in a reduction in the electronic oscillations [31]. Some resonance peaks emerged on the permittivity spectra at high GS loadings, which are usually observed when the material is highly conductive [32]. The highest ϵ' and ϵ'' values with 6.0 wt% GS loadings were in the ranges of 21.4–26.1, 17.9–18.3 respectively. These are better than or close to those of graphene–polymer composites in the X-band with similar filler loadings [33, 35]. The GS/PA composites had $\epsilon'(\epsilon'') \sim 4(7)$ times greater than those of GF/PA composites (figures 5(a), (b)). The high permittivity of the GS/PA composites implied strong interactions between the GS/PA composites and microwaves in the X-band. The macroscopic permittivity of composite materials is complex and depends on many factors such as the shape, persistence length, conductivity, and the interfacial polarization [36, 37]. For the non-magnetic graphene–polymer system, Maxwell–Wagner–Sillars (MWS) polarization is regarded as an essential factor influencing the real permittivity (ϵ') in the GHz range. According to the MWS principle, the disparity between the conductivities of two adjacent materials results in polarization and charge accumulation at their interfaces. Here, GS were incorporated in the PA matrix through a latex mixing process and a

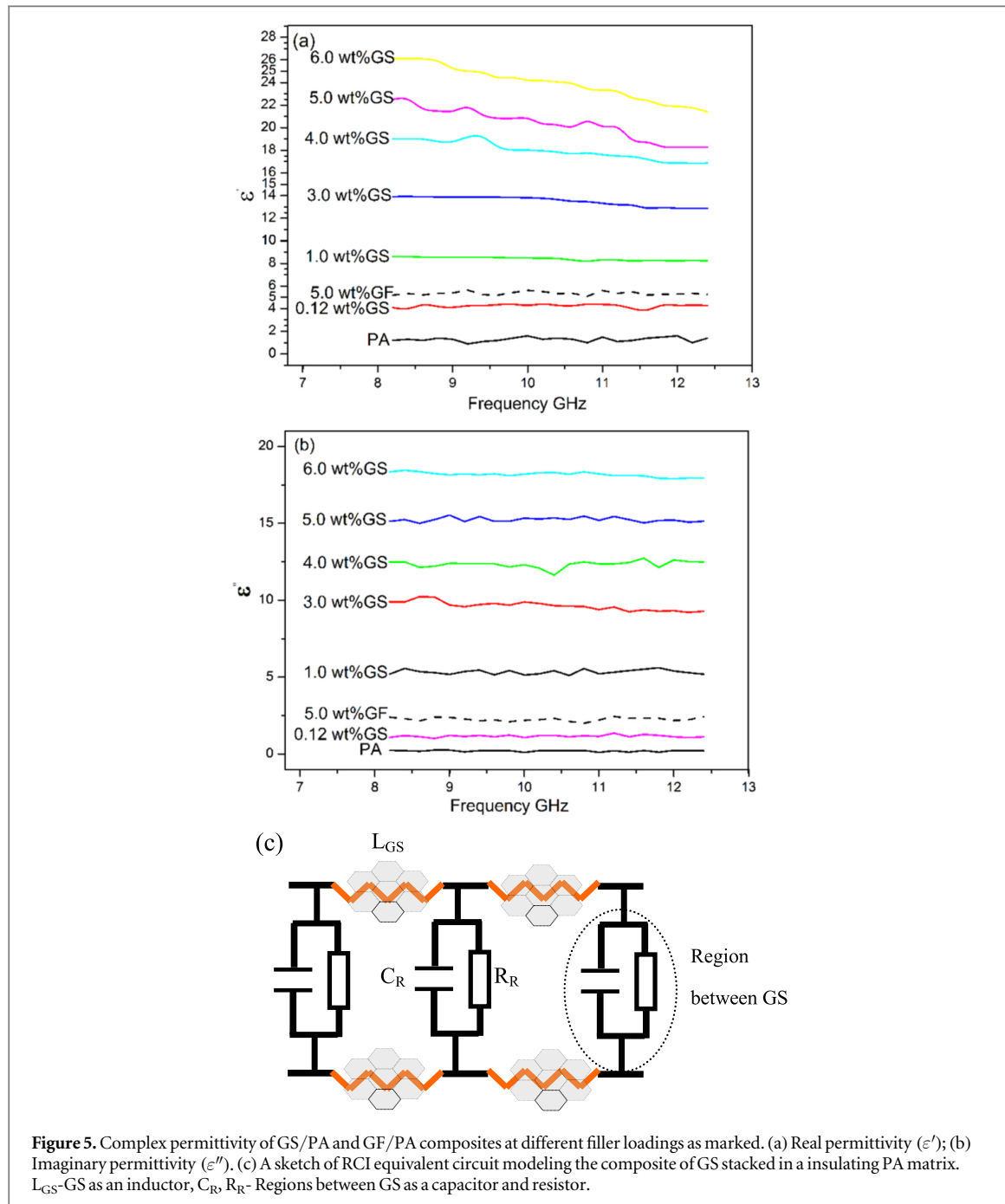


Figure 5. Complex permittivity of GS/PA and GF/PA composites at different filler loadings as marked. (a) Real permittivity (ϵ'); (b) Imaginary permittivity (ϵ''). (c) A sketch of RCI equivalent circuit modeling the composite of GS stacked in a insulating PA matrix. L_{GS} -GS as an inductor, C_R , R_R - Regions between GS as a capacitor and resistor.

heterogeneous system (the segregated GS architecture and PA matrix) was formed, having different conductivities, σ_1 and σ_2 , and dielectric constants, ϵ'_1 and ϵ'_2 , respectively. As a result, strong interfacial polarization appears due to the ultra-large disparity between the two media in the applied microwave electromagnetic field. The adjacent parallel GS separated by an insulating PA layer can serve as a mini-capacitor, where the polar bonds or charges tend to align in the electromagnetic field, favorable for polarization [34]. The composite in microwave electromagnetic field can be described by an equivalent resistor-capacitor-inductor (RCI) circuit model, where the GS represent an inductor (L_{GS}) due to their highly conductive nature, and the contact regions between GS represent a capacitor and resistor (R_C , R_R) (figure 5(c)). The as-prepared GS, which have higher aspect ratios than those of GF, could provide millions of mini-capacitors to store electric charges in the non-conductive PA matrix, enabling the conductive composite to possess a higher real permittivity (ϵ'). Moreover, the excellent hexagonal graphene framework cannot be completely preserved and defects such as missing carbon atoms and sheet corrugation were introduced after a wet grinding process. According to the literature, localized states near the Fermi level can be constructed by introducing lattice defects, which can contribute to electromagnetic energy absorption by the transition from continuous states to Fermi level

irradiated by electromagnetic wave [36]. Therefore, compared with the GF/PA composites, the improved aspect ratios coupled with lattice defects on the GS are responsible for the dramatic enhancement of the real permittivity (ϵ'). The imaginary permittivity is a measure of the dissipated energy due to electric loss for a graphene–polymer system, and electrical conductivity is a highly significant factor for influencing the imaginary permittivity (ϵ'') in dielectric loss dominated materials [34]. According to the dc conductive results, the GS/PA composites exhibited higher conductivity and lower percolation threshold value than that of GF/PA composites. As a result, the improved electrical conductivity of the GS/PA composites makes the main contribution to the enhancement of the imaginary permittivity (ϵ'') of the GS/PA composites.

EMI shielding performance

Electromagnetic shielding is a process whereby the flow of electromagnetic field is limited between two locations, by separating them with a barrier made of conducting materials. The SE is defined as a measure of the attenuation of incident electromagnetic radiation by a particular material and is expressed in decibels (dB). According to the shielding theory, there are three mechanisms in the shielding process, namely reflection loss (SE_R), absorption loss (SE_A) and multiple reflections loss (SE_M). Reflection loss is correlated with the mobile charge carriers in the composites which can interact with the incident EM radiation. EM radiation attenuated by absorption originates from generation of eddy currents and requires electric and/or magnetic dipoles in the material. The multiple reflection loss is related with the interfaces in materials and can be ignored when the total SE is larger than 15 dB.

The total SE is the sum of reflection, absorption and multiple loss and can be expressed as:

$$SE_{\text{total}} = SE_R + SE_A + SE_M. \quad (3)$$

Minimum SE_{total} of 20 dB is required for applications, indicating 99% of EM radiation is blocked, and for military applications, the required minimum SE_{total} is 30 dB.

When an EM wave passes through a conductive material, its amplitude decreases exponentially with the depth of the material. The depth at which electromagnetic energy decreases to $1/e$ of the incident wave, is known as skin depth (δ). For conductive materials, the skin depth can be calculated as:

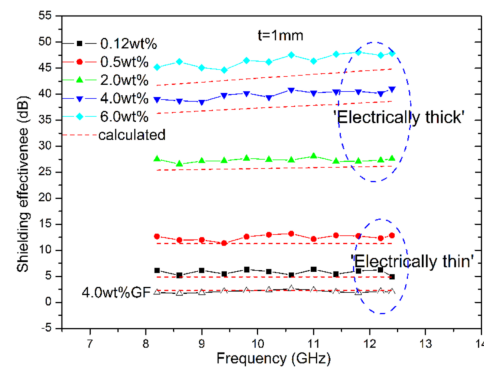
$$\delta = \frac{1}{\sqrt{\pi f \mu \sigma}} \quad (4)$$

Where $\mu = \mu_0 \mu_r$, $\mu_0 = 4\pi \times 10^{-7} \text{ Hm}^{-1}$ and σ are magnetic permeability and conductivity, respectively, of the shielding material and f is frequency. For the nonmagnetic GS/PA composite systems, we have $\mu_r = 1$.

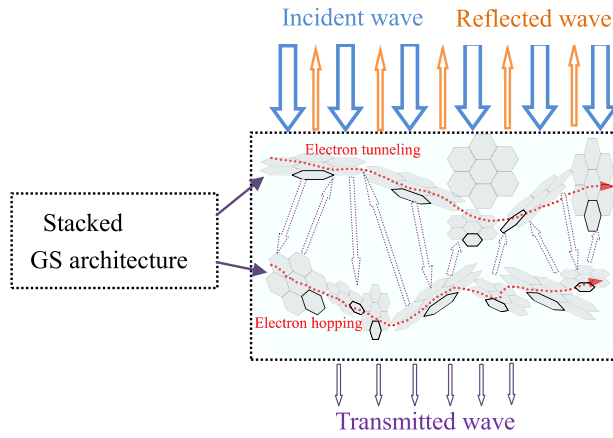
According to classical EM wave theory, EM radiation can be divided into far field ($r \gg \lambda/2\pi$, where λ is EM radiation wavelength and r is the distance from the radiation source to the shield) and near field ($r \ll \lambda/2\pi$). In this paper, the distance (1 m) is far more than the wavelength of X-band (3.65–0.24 cm wavelength), therefore, only shielding performances in far field are considered.

As discussed earlier, the remarkable enhancement of conductivity and complex permittivity potentially endowed the GS/PA composites with excellent EMI SE property to block unwanted EM noises. Figure 6(a) showed the SE variations of composites with increasing GS content at $t = 1 \text{ mm}$. The concrete panel with neat PA polymer was almost transparent to electromagnetic waves and exhibited poor shielding capacity ($\sim 0.5 \text{ dB}$, not shown) because of the insulating nature of PA and slight ionic conduction of the concrete panel. The SE of GS/PA composites increased with increasing GS content, and they all showed little fluctuation over the whole frequency range for a given GS content, exhibiting excellent frequency stability in the X-band. The EMI SE values of 0.12 and 0.5 wt% GS in composites were found to be ≈ 5 and $\approx 11 \text{ dB}$ respectively, in X-band. Similarly, exceptional EMI SE values of ≈ 38 and $\approx 44 \text{ dB}$ have been delivered for 4 and 6 wt % GS respectively, which indicated only 0.016 and 0.004% EM transmission through the GS/PA composites. In contrast, the EMI SE of GF/PA composite was found to be very low, at $\approx 2 \text{ dB}$ in X-band for 4 wt% GF. The low conductivity and permittivity of GF resulted in inferior EMI shielding performance. Clearly, the dominant contribution to the EMI shielding performances of GS/PA composites can be assigned to the formation of a conductive network consisting of segregated GS architecture stacked in the insulating PA matrix. As a continuous conductive network is formed beyond the percolation threshold (0.11 wt% GS), the EMI SE of the GS/PA increased dramatically with the increase of conductivity and GS concentrations. The enhanced EMI shielding performance can also be explained in terms of reduction of the skin depth due to the increase of conductivity. The skin depth decreased with increasing GS concentrations and frequency (figure 3(S)), which made it possible to achieve the same level of SE with a thinner shield. The material with the thinnest skin depth was expected to give the maximum EMI SE values at the same thickness. Therefore, for a given thickness (1 mm), the EMI shielding performances increased greatly with the decreased skin depth of the GS/PA composite.

Further theoretical investigation on the EMI shielding of GS/PA composites was conducted based on the plane-wave theory under the assumption that the prepared GS/PA composite is an infinite isotropic and good



(a)



(b)

Figure 6. (a) SE variations of GS/PA and GF/PA composites with different filler loadings at $t = 1$ mm (numbers in % indicate mass fraction of GS). (b) Schematic representation of microwave transfer across the GS/PA composite segregated GS architecture.

conductor. The expression of the SE_{total} in far field can be simplified depending on the relative value of the thickness of the sample (t) compared to the skin depth (δ).

When $t/\delta < 1.3$, the samples can be regarded as ‘electric thin’, the SE_{total} can be expressed by a function of conductivity (σ), sample thickness (t), as follows [8, 38]:

$$SE(\text{dB}) = 20 \log\left(1 + \frac{Z_0 t \sigma}{2}\right) \quad (5)$$

When $t/\delta \geq 1.3$ the tested sample can be regarded as ‘electric thick’, SE_{total} can be expressed as follows:

$$SE(\text{dB}) = 20 \log\left(\frac{Z_0 \delta \sigma}{2\sqrt{2}}\right) + 8.68 \frac{t}{\delta} \quad (6)$$

Where $Z_0 = 120\pi$ is the impedance of free space.

Theoretical calculations of EMI SE based on equations (5) and (6) were carried out in X-band in far field. The above equations for SE calculations are widely used and fitted for carbon based composites [8, 38, 39]. For the composites with 0.12 and 0.5 wt% GS and 4 wt% GF content, the values of t/δ were less than 1.3 in X-band (figure S3), indicating the composites were ‘electrically thin’, therefore, equation (5) was used to calculate the SE_{total} . When the GS content increased to 2 wt%, the values of t/δ were larger than 1.3, the composites transformed from ‘electrically thin’ to ‘electrically thick’, and equation (6) was used to calculate the SE_{total} . The calculated results were shown in figure 6(a) by red dash shots. The calculated SE values provided excellent agreements with the measured SE for the composite containing 4 wt% GF, taking into account that the measured SE values were affected by oscillation and resonance due to the imperfect electrical contacts between the samples and the aperture. The above agreement confirmed that the prepared GF/PA composites were isotropic and good conductors. The measured values of SE for GS/PA composites were larger than the calculated ones. The difference was ~ 2 dB at low GS loadings (0.12 ~ 0.5 wt% GS) and increased to ~ 4 dB at high GS loadings (4 ~ 6 wt% GS). The sharper difference between the measured and calculated EMI SE suggested important structural and material characteristics of the GS and prepared composites, including high intrinsic

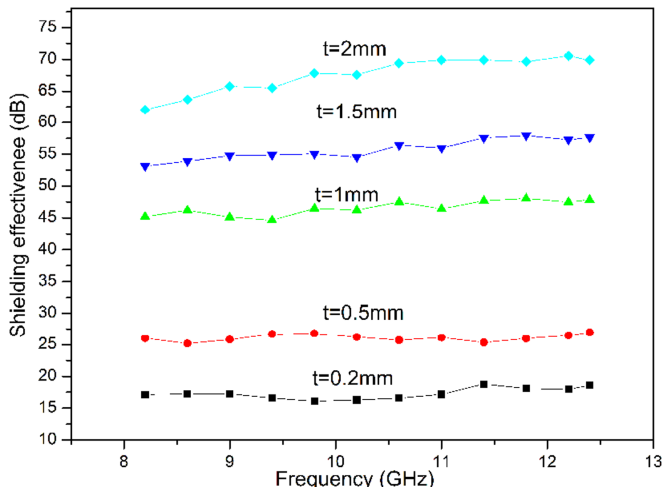


Figure 7. EMI SE as a function of frequency for the GS/PA composites with various thicknesses.

conductivity and dielectric constant, large aspect ratios of GS, and the segregated architecture of GS in the PA matrix.

There are two reasons for the above SE differences of GS/PA composites. Firstly, the segregated architecture of GS can be considered as highly conductive ‘membranes’ in the PA matrix, and the deformed PA spheres covered by GS led to a great number of membranes. The large heterogeneous interfaces provided by the extremely thin, flexible and corrugated GS in PA matrix were beneficial for the multiple reflecting and scattering of EM waves due to its excellent conductivity, and consequently for the additional absorption-dominant EMI shielding [40, 41]. The incident EM waves were attenuated by reflecting, scattering and adsorption many times by the multiple layers of conductive GS membranes, and it was very difficult for EM waves to penetrate the composite (figure 6(b)).

Secondly, the SE calculation was based on the good conductor approximation and reflection loss was the main mechanism of EMI shielding. It is well accepted in literature that adsorption attenuation is the dominant shielding mechanism for graphene–polymer composites, whereby electric dipoles in the shield interact with the electromagnetic fields while radiation passes through the shield [28, 29]. The highly conductive and dielectric GS/PA composites had high charge storage capacities and could lead to strong coupling between the well-stacked GS architecture and microwaves. The segregated architecture of GS with high aspect ratios and intrinsic conductivity favors electron hopping and tunneling in the PA matrix (figure 6(b)), As a result, the high frequency EM waves are trapped by the resistor-capacitor-inductor (RCI) network in the composites (figure 6(c)) and strongly attenuated by dielectric loss.

It is well established that the EMI SE increases with increasing specimen thickness. The effect of thickness on EMI SE of the composites with 6 wt% GS was investigated, as shown in figure 7. Clearly, the EMI SE of the composites depended on the sample thickness. A significant increase of the EMI SE can be found from ~16 dB to ~66 dB in X-band when the sample thickness increased from 0.2 to 2.0 mm and a maximal EMI SE of 70 dB was achieved for composite containing 6 wt% GS. The composite with the thickness of 0.5 mm exhibited an EMI SE of ~25 dB and thus the critical thickness for the GS/PA composites to show shielding properties (exceed 20 dB) should be in the vicinity of 0.5 wt% GS. The enhancement of the shielding thickness led to an increased amount of GS architecture in the PA matrix, which can provide more interfaces to interact with incident EM microwaves.

Table 1 compared the EMI SE and filler concentrations between various shielding materials reported in literature. The EMI SE of the GS/PA composites in current work have been greatly improved compared with previously reported graphene-based composites, at similar thickness and similar or even lower GS loadings. The GS were selectively distributed at the interfaces of deformed PA spheres, instead of being uniformly distributed throughout the whole PA matrix. This localized distribution can greatly increase the utilization ratio of GS, leading to reduced GS loadings. Moreover, segregated architecture of GA in the PA matrix can effectively interact with incident radiation, resulting in a very high EMI SE.

Table 1. EMI shielding properties for different graphene-based composites.

Polymer	Graphene concentration (wt/vol%)	Sample thick- ness (mm)	Frequency range (GHz)	EMI SE (dB)	Ref.
PA	6	2	8.2–12.4	67	Present work
PMMA ^{a)}	8	3.4	8.2–12.4	30	[13]
Epoxy	15	2	8.2–12.4	21	[14]
WPU ^{a)}	7.7	2.0	8.2–12.4	33	[15]
WPU ^{a)}	5	2.0	8.2–12.4	38	[17]
PS ^{a)}	7	2.5	8.2–12.4	45.1	[42]
PS ^{a)} foam	30	2.5	8.2–12.4	29	[43]
PEI foam ^{a)}	10(graphene @Fe ₃ O ₄)	2.5	8.2–12.4	18	[44]
PDMS ^{a)} foam	0.8	3	8.2–12.4	34	[45]
UHMWPE ^{a)}	0.065	2.5	8.2–12.4	28.3–32.4	[46]
PVA ^{a)}	6(plus 2.0Fe ₂ O ₃)	0.36	8.2–12.4	20.3	[47]

PS, WPU, PMMA PDMS, UHMWPE, PVA, PEI are polystyrene, waterborne polyurethane, poly(methyl methacrylate), poly(dimethyl siloxane), ultrahigh molecular weight polyethylene, poly(vinyl alcohol) and polyetherimide, respectively.

Conclusions

In summary, we have stacked a segregated architecture of GS in a PA matrix by a latex mixing process to prepare a highly efficient EMI attenuation polymer composite with low active filler loading. The GS were prepared by a mechanical delamination process in water from GF. A remarkably low percolation threshold of ~0.11 mass per cent for room-temperature electrical conductivity was obtained in the GS/PA composite owing to the segregated architecture of GS with high aspect ratios. This unique nanostructured GS architecture not only enhanced the electrical conductivity of composites, but also dramatically increased complex permittivity by inducing strong MWS polarization at the conductive GS/non-conductive PA interfaces. The EMI SE of these composites were enhanced with the increase of GS content and the composite with 6 wt% loading exhibited a high EMI SE of ~66 dB over a frequency of 8.2–12.4 GHz, resulting from the pronounced conduction loss, dielectric relaxation, and multi-scattering. These results demonstrated a promising green approach to fabricate an ultra-efficient electromagnetic interference (EMI) shielding material against electromagnetic pollution, due to its environmentally friendly preparation process.

Acknowledgments

This work was supported by the International Science and Technology Cooperation Program of China (No.2014DFR51010), External Cooperation Program of Chinese Academy of Sciences (No.GJHZ201310), National Natural Science Foundation of China (Nos.51372255, 51422211, 51432004) and Beijing Natural Science Foundation (No. 2131006). This work is partially funded by the Key Laboratory of Cryogenics, Technical Institute of Physics and Chemistry, Chinese Academy of Sciences.

Competing financial interests

The authors declare no competing financial interests.

Author contributions

Y L conceived the experimental design and performed the electromagnetic shielding testing experiments and calculations. Z S conducted the characterization with SEM and TEM. X L performed the characterization with AFM. Y N conducted the dc conductivity experiment. All the authors discussed the results and contributed to preparing the manuscript.

References

- [1] Wen B *et al* 2014 Reduced graphene oxides: light-weight and high-efficiency electromagnetic interference shielding at elevated temperatures *Adv. Mater.* **26** 3484
- [2] Zhang Y *et al* 2015 Broadband and tunable high-performance microwave absorption of an ultralight and highly compressible graphene foam *Adv. Mater.* **27** 2049
- [3] Saini P *et al* 2013 High permittivity polyaniline–barium titanate nanocomposites with excellent electromagnetic interference shielding response *Nanoscale* **5** 4330

- [4] Lin C T *et al* 2003 Nanograin magnetoresistive manganite coatings for EMI shielding against directed energy pulses *Prog. Org. Coat.* **47** 190
- [5] Lipman R M *et al* 1988 Cataracts induced by microwave and ionizing radiation *Surv. Ophthalmol.* **33** 200
- [6] Elder J A *et al* 2003 Ocular effects of radiofrequency energy *Bioelectromagnetics* **24** S148
- [7] <http://who.int/peh-f/about/WhatisEMF/en/index1.html>
- [8] Zhou H *et al* 2013 Synthesis and electromagnetic interference shielding effectiveness of ordered mesoporous carbon filled poly(methyl methacrylate) composite films *RSC Advances* **3** 23715
- [9] Thomassin J M *et al* 2013 Polymer/carbon based composites as electromagnetic interference (EMI) shielding materials *Mater. Sci. Eng. R* **74** 211
- [10] Whitby R L D 2014 Chemical control of graphene architecture: tailoring shape and properties *ACS Nano* **8** 9733–9754
- [11] Chen C *et al* 2015 Graphene nanoribbons under mechanical strain *Adv. Mater.* **27** 303
- [12] Yousefi N *et al* 2014 Highly aligned graphene/polymer nanocomposites with excellent dielectric properties for high-performance electromagnetic interference shielding *Adv. Mater.* **26** 5480
- [13] Zhang H B *et al* 2012 The effect of surface chemistry of graphene on rheological and electrical properties of polymethylmethacrylate composites *Carbon* **50** 5117
- [14] Liang J *et al* 2009 The effect of surface chemistry of graphene on rheological and electrical properties of polymethylmethacrylate composites *Carbon* **47** 922
- [15] Hsiao S T *et al* 2013 Using a non-covalent modification to prepare a high electromagnetic interference shielding performance graphene nanosheet/water-borne polyurethane composite *Carbon* **60** 57
- [16] Maiti S *et al* 2013 Polystyrene/MWCNT/graphite nanoplate nanocomposites: efficient electromagnetic interference shielding material through graphite nanoplate–MWCNT–graphite nanoplate networking *ACS Appl. Mater. Interfaces* **5** 4712
- [17] Hsiao S T *et al* 2015 Effect of covalent modification of graphene nanosheets on the electrical property and electromagnetic interference shielding performance of a water-borne polyurethane composite *ACS Appl. Mater. Interfaces* **7** 2817
- [18] Nöl A *et al* 2014 Tunable architecture for flexible and highly conductive graphene–polymer composites *Compos. Sci. Technol.* **95** 82
- [19] Regev O *et al* 2004 Preparation of conductive nanotube–polymer composites using latex technology *Adv. Mater.* **16** 248
- [20] Hao G *et al* 2015 Investigation on the film surface and bulk properties of fluorine and silicon contained polyacrylate *Prog. Org. Coat.* **85** 8
- [21] Kyrylyuk A V *et al* 2011 Controlling electrical percolation in multicomponent carbon nanotube dispersions *Nat. Nanotech.* **10** 1
- [22] Nicolson A M *et al* 1970 Measurement of the intrinsic properties of materials by time domain techniques *IEEE Trans. Instrum. Meas.* **19** 377
- [23] Pham V H *et al* 2012 Highly conductive poly(methyl methacrylate) (PMMA)-reduced graphene oxide composite prepared by self-assembly of PMMA latex and graphene oxide through electrostatic interaction *ACS Appl. Mater. Interfaces* **4** 2630
- [24] Stankovich S *et al* 2006 Graphene-based composite materials *Nature* **442** 282
- [25] Zhang H B *et al* 2010 Electrically conductive polyethylene terephthalate/graphene nanocomposites prepared by melt compounding *Polymer* **51** 1191
- [26] Yoonessi M *et al* 2010 Highly conductive multifunctional graphene polycarbonate nanocomposites *ACS Nano* **4** 7211
- [27] Kim H M *et al* 2004 Electrical conductivity and electromagnetic interference shielding of multiwalled carbon nanotube composites containing Fe catalyst *Appl. Phys. Lett.* **84** 589
- [28] Noël A *et al* 2014 Electrical and mechanical percolation in graphene-latex nanocomposites *Polymer* **55** 5140
- [29] Chung D L *et al* 2004 Electrical applications of carbon materials *J. Mater. Sci.* **39** 2645
- [30] Bai X *et al* 2011 Green approach to prepare graphene-based composites with high microwave absorption capacity *J. Phys. Chem. C* **115** 11673
- [31] Panwar V *et al* 2008 Analysis of electrical, dielectric, and electromagnetic interference shielding behavior of graphite filled high density polyethylene composites *Polym. Eng. Sci.* **48** 2178
- [32] Che R C *et al* 2004 Microwave absorption enhancement and complex permittivity and permeability of Fe encapsulated within carbon nanotubes *Adv. Mater.* **16** 401
- [33] D'Aloia A G *et al* 2014 Electromagnetic absorbing properties of graphene–polymer composite shields *Carbon* **73** 175
- [34] Song W L *et al* 2013 Improved dielectric properties and highly efficient and broadened bandwidth electromagnetic attenuation of thickness-decreased carbon nanosheet/wax composites *J. Mater. Chem. C* **1** 1846
- [35] Wen B *et al* 2014 Reduced graphene oxides: the thinnest and most lightweight materials with highly efficient microwave attenuation performances of the carbon world *Nanoscale* **6** 5754
- [36] Wang C *et al* 2011 The electromagnetic property of chemically reduced graphene oxide and its application as microwave absorbing material *Appl. Phys. Lett.* **98** 072906
- [37] Yu S *et al* 2000 Dielectric properties of polystyrene–aluminum-nitride composites *J. Appl. Phys.* **88** 398
- [38] Zhang C S *et al* 2007 Electromagnetic interference shielding effect of nanocomposites with carbon nanotube and shape memory polymer *Compos. Sci. Technol.* **67** 2973
- [39] Li Y *et al* 2010 Enhanced dielectric constant for efficient electromagnetic shielding based on carbon-nanotube-added styrene acrylic emulsion based composite *Nanoscale. Res. Lett.* **5** 1170
- [40] Al-Saleh M H *et al* 2009 Electromagnetic interference shielding mechanisms of CNT/polymer composites *Carbon* **47** 1738–46
- [41] Yan D X *et al* 2015 Structured reduced graphene oxide/polymer composites for ultra-efficient electromagnetic interference shielding *Adv. Funct. Mater.* **25** 559
- [42] Yan D X *et al* 2012 Efficient electromagnetic interference shielding of lightweightgraphene/polystyrene composite *J. Mater. Chem.* **22** 18772
- [43] Zhang H B *et al* 2011 Tough graphene-polymer microcellular foams for electromagnetic interference shielding *ACS Appl. Mater. Interfaces* **3** 918
- [44] Shen B *et al* 2013 Lightweight, Multifunctional polyetherimide/Graphene@Fe₃O₄ composite foams for shielding of electromagnetic pollution *ACS Appl. Mater. Interfaces* **5** 11383
- [45] Chen Z *et al* 2013 Lightweight and flexible graphene foam composites for high-performance electromagnetic interference shielding *Adv. Mater.* **25** 1296
- [46] Yan D X *et al* 2014 Electromagnetic interference shielding of segregated polymer composite with an ultralow loading of *in situ* thermally reduced graphene oxide *Nanotechnology* **25** 145705
- [47] Yuan B *et al* 2014 Design of artificial nacre-like hybrid films as shielding to mitigate electromagnetic pollution *Carbon* **75** 178